Modal dynamics in multimode fibers

Moti Fridman,[†,*] Haim Suchowski,[†] Micha Nixon, Asher A. Friesem, and Nir Davidson

Weizmann Institute of Science, Department of Physics of Complex Systems, Rehovot 76100, Israel
**Corresponding author: mf557@cornell.edu*

Received August 22, 2011; revised December 14, 2011; accepted January 11, 2012;
posted January 12, 2012 (Doc. ID 153267); published March 22, 2012

The dynamics of modes and their states of polarizations in multimode fibers as a function of time, space, and wavelength are experimentally and theoretically investigated. The results reveal that the states of polarizations are displaced in Poincaré sphere representation when varying the angular orientations of the polarization at the incident light. Such displacements, which complicate the interpretation of the results, are overcome by resorting to modified Poincaré sphere representation. With such modification it should be possible to predict the output modes and their state of polarization when the input mode and state of polarization are known.

OCIS codes:: 260.5430, 060.2310.

1. INTRODUCTION

Multimode fibers have high coupling efficiencies, can operate over a wide range of wavelengths, and have relatively low susceptibility to degrading nonlinear effects. As a result, they are widely used in mid and short communication ranges, high power lasers and amplifiers, and in transporting high optical powers from one location to another [1,2]. Yet, while in single mode fibers the polarization dispersion is low and can be significantly reduced either by using polarization maintaining fibers or by operating at the principal state of polarization [3–9], in multimode fibers the mode dispersion is high, resulting in significant reduction of performance [10,11]. Consequently, it is important to continuously analyze and monitor the dynamics of the modes propagating in multimode fibers.

When analyzing the dynamics of modes in multimode fibers, it is common to separate the dynamics of the transverse modes and the dynamics of the states of polarization [12–16]. Unfortunately, since there is coupling between transverse modes with different states of polarization, such a separation is not natural and results in coupled equations that are difficult to analyze. Here we present a new approach where the complicated dynamics of the modes in multimode fibers are separated and represented by two uncoupled equations of motion that lead to simple geometric plots on modified and uncoupled Poincaré spheres. Such plots fully describe the modal dynamics in multimode fibers, and can be conveniently used for monitoring, analyzing and predicting them.

We begin by describing our experimental configuration and present experimental results of the state of polarization (SOP) at the output from multimode fiber as a function of wavelength for different angular orientations of light with linear polarization at the input. The results reveal that the dynamics of the modes and their SOP at the output from multimode fibers are relatively complicated. Then we developed an analytical model for calculating these dynamics and show how their representation can be simplified to obtain a more convenient and intuitive understanding. Finally, based on the results from the model, we show how to obtain such simplified representation experimentally.

2. EXPERIMENTAL CONFIGURATION AND RESULTS

The experimental configuration for measuring the output polarization from a multimode fiber is presented in Fig. 1. A linearly polarized light from a tunable fiber laser propagates through a half wave plate and a quarter wave plate in order to obtain light of any desired SOP and wavelength at the input. The light is then launched into a multimode fiber, and the SOP at the output as a function of space, time, and wavelength is measured using a real-time space-variant polarization measurement system [17]. In our experiments the multimode fiber length was 10 m, core diameter 13 μm, and numerical aperture 0.07. It mainly supported the TE_{01} and TM_{01} modes, which in the weakly guided approximation can be expressed as orthogonal sets of linearly polarized modes. The electric field intensity distributions and polarization directions for these modes are presented in Fig. 2. As shown, there are four distinct modes of LP_{11}, each with different intensity distribution or different orientations of the polarization direction. The white arrows at the center of the individual intensity distributions denote the direction of the polarizations in each mode. Our fibers have a special index of refraction profile that favors the LP_{11} modes over the LP_{01} mode [18,19].

We started our experiments by verifying that the coupling into the fiber does not change the mode or the SOP of the input. This was done by determining that the intensity distribution of the mode and the SOP at the output are the same as those at the input after propagating through a short 7 cm fiber. Then, we launched the same linearly polarized light with a uniform intensity distribution into the 10 m long fiber and measured the SOP at the output while varying the input wavelength from 1062 nm to 1066 nm. We repeated these measurements, each time after rotating the linearly polarized light at the input by 10°.

The results are presented in Fig. 3 as a Poincaré sphere representation of the SOP at the output for different angular orientations of the linear polarization at the input. The SOP

[†]These authors contributed equally to this work.

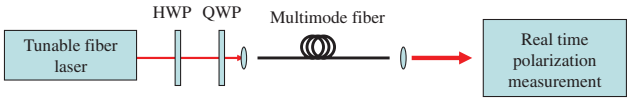

Fig. 1. (Color online) Experimental configuration for measuring the output polarization from a multimode fiber as a function of the input wavelength for different input states of polarization.

as a function of wavelength essentially fall along the circumference of circles. As evident, the circle of smallest size is obtained when the linearly polarized input beam is oriented at 30°, indicating where the SOP of the output is nearly invariant to the input wavelengths. Namely, at an angular orientation of about 30°, we are close to the principal mode (PM). As the deviation from 30° increases, the circles become larger, indicating that more spectral dispersion occurs. Unlike increasing concentric circles around the principal state of polarization location in single mode fiber, here we obtained increasing circles whose centers continuously deviate from the PM location as the difference between the input and the PM increases. We also present the projection of the output polarization on the S_1 axes as a function of the input wavelength for two input polarization in Fig. 4. As evident, when the input polarization is close to the PM the output polarization is less sensitive to wavelength variations. We performed the same experiments also for input linear polarization from −90 to 0 degrees and obtained similar results. All our experiments were done in a controlled environment and during a short period of time so the PM remains constant.

3. MODEL AND CALCULATED RESULTS

We developed a model for calculating the dynamics of the SOP at the output of multimode fibers, in order to gain a better physical intuition about the evolution of modes in a multimode fiber and to understand what causes the deviations from the PM location. We define E_{in} and E_{out} as the input and output modes composed from a superposition of the four fields $E_{\text{in,out}} = [E_1, E_2, E_3, E_4]^T_{\text{in,out}}$, shown in Fig. 2. The relation between them is $E_{\text{out}} = e^{i\beta}\mathbf{U}E_{\text{in}}$, where β is real and $\mathbf{U}$ is a unitary matrix so $\mathbf{U}(\omega) = \exp(\mathbf{H})$, where $\mathbf{H}$ is skew-Hermitian matrix. In order to analyze the dynamics of modes as a function of the input wavelength, we differentiated the relation between E_{out} and E_{in} with respect to frequency, and used the definition of $\mathbf{U}$ to obtain

$$\frac{dE_{\text{out}}}{d\omega} = \mathbf{H}E_{\text{out}}. \tag{1}$$

To explicitly define $\mathbf{H}$, we assume that birefringence and twists in the fiber are the main sources for coupling between the modes. Birefringence in the fiber leads to coupling of modes with the same intensity distributions but with orthogonal SOP. Accordingly, the coupling between the fields E_1 and E_2 can be described by a 2 by 2 matrix, as

$$\mathbf{H}^{(2)}(\omega) = \begin{bmatrix} h_1(\omega) & h_2(\omega) \\ -h_2^*(\omega) & h_1^*(\omega) \end{bmatrix}, \tag{2}$$

where h_1 is purely imaginary and denotes changes in the phase of each mode, and h_2 denotes the coupling strength between the modes while propagating in the fiber. Similarly, since E_3 and E_4 also have the same intensity distributions and assuming that birefringence is essentially constant across

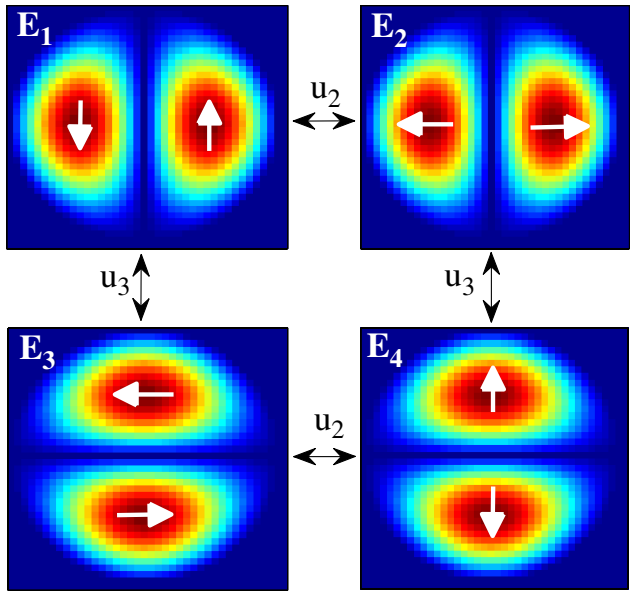

Fig. 2. (Color online) Intensity distributions together with the orientations of the polarization direction for the orthogonal sets of linearly polarized modes LP_{11}. The white arrows in the center of the individual intensity distributions denote the polarization directions. The black arrows and the terms u_2 and u_3 denote the coupling between the different modes.

a relatively small fiber core [20,21], we can describe the coupling between E_3 and E_4 with the same unitary matrix $H^{(2)}(\omega)$. Twists in the fiber rotate the modes and lead to coupling between E_1 and E_3 and between E_2 and E_4 with coupling strength denoted as h_3. We also assume that coupling between E_1 and E_4 and between E_2 and E_3 are negligible. The overall coupling matrix between all four fields is then

$$\mathbf{H}(\omega) = \begin{bmatrix} h_1(\omega) & h_2(\omega) & h_3(\omega) & 0 \\ -h_2^*(\omega) & h_1^*(\omega) & 0 & h_3(\omega) \\ -h_3^*(\omega) & 0 & h_1(\omega) & h_2(\omega) \\ 0 & -h_3^*(\omega) & -h_2^*(\omega) & h_1^*(\omega) \end{bmatrix}. \tag{3}$$

Using Pauli matrices, σ_x, σ_y, and σ_z, we can decompose $\mathbf{H}$ to

$$\mathbf{H} = (ib_1\sigma_z + ia_2\sigma_y + ib_2\sigma_x) \otimes I + I \otimes (ib_3\sigma_x + ia_3\sigma_y), \tag{4}$$

where a_i denote the real part of h_i and b_i the imaginary part of h_i. Equation (4) defines rotation in four dimensions, one part for left rotation and the other for right rotation [22,23]. Now, in order to find analytic solution to Eq. (1), we redefine the vectors E_{in} and E_{out} to a 2 by 2 matrices,

$$\tilde{E}_{\text{in,out}} = \begin{bmatrix} E_1 & E_2 \\ E_3 & E_4 \end{bmatrix}_{\text{in,out}}, \tag{5}$$

and using Eqs. (4) and (5) leads to the solution of $\tilde{E}_{\text{out}}$ as a function of frequency as

$$\tilde{E}_{\text{out}}(\omega) = \mathbf{\Omega}_L(\omega)\tilde{E}_{\text{in}}\mathbf{\Omega}_R(\omega), \tag{6}$$

where

$$\mathbf{\Omega}_L(\omega) = \begin{bmatrix} \cos(|\tau_b|\omega) & \frac{\tilde{u}_3}{|\tau_b|}\sin(|\tau_b|\omega) \\ -\frac{\tilde{u}_3^*}{|\tau_b|}\sin(|\tau_b|\omega) & \cos(|\tau_b|\omega) \end{bmatrix} \tag{7}$$

and

$$\mathbf{\Omega}_R(\omega)=\begin{bmatrix}\cos(|\tau_a|\omega)+\frac{\tilde{u}_1}{|\tau_a|}\sin(|\tau_a|\omega) & \frac{-\tilde{u}_2^*}{|\tau_a|}\sin(|\tau_a|\omega)\\ \frac{\tilde{u}_2}{|\tau_a|}\sin(|\tau_a|\omega) & \cos(|\tau_a|\omega)-\frac{\tilde{u}_1}{|\tau_a|}\sin(|\tau_a|\omega)\end{bmatrix}$$

with $\tau_a \equiv (b_1, b_2, a_2)$ and $\tau_b \equiv (0, a_3, b_3)$.

Equation (6) provides an analytic solution of the output mode distribution and its SOP as a function of the wavelength when the input SOP is known. It involves a multiplication of two matrices $\mathbf{\Omega}_R$ and $\mathbf{\Omega}_L$. The matrix $\mathbf{\Omega}_R$ is composed from u_1 and u_2 so it represents the coupling between each pair of modes with the same intensity distributions but with different SOP, whereas the matrix $\mathbf{\Omega}_L$ is composed only from u_3, so it represents the coupling between each pair of modes with different intensity distributions and different SOP. Using Eq. (6), we calculated the evolution of the output SOP as a function of the input wavelength for different angular orientations of a linearly polarized light at the input. The results are presented in Fig. 3, with the coupling parameters u_1, u_2, and u_3 as fit parameters. As evident, there is a qualitative agreement between the experimental and calculated results, indicating that our assumptions in developing the model are justified. We evaluated the difference between the experimental results and ellipse and found it to be less than 10%. We attribute the small difference between the calculated results and the measured results to small errors in our polarization measurement and to the existence of additional transverse modes in the fiber and additional coupling terms beyond those used in our model. The value for the coupling strength in the calculated results is $u_2 = 0.1 + 0.1i$, $u_3 = -2 + 3i$ and the detuning, u_1, is less than 0.1.

4. MODIFIED POINCARÉ SPHERE REPRESENTATION

In order to simplify the Poincaré sphere representation of the SOP dynamics at the output, we resorted to modified Stokes parameters $S_a \equiv (S_a^{(1)}, S_a^{(2)}, S_a^{(3)})$ and $S_b \equiv (S_b^{(1)}, S_b^{(2)}, S_b^{(3)})$, where

$$\begin{aligned}S_a^{(1)} &= |E_1|^2 - |E_2|^2 + |E_3|^2 - |E_4|^2\\ S_a^{(2)} &= 2|E_1||E_2|\cos(\varphi_{12}) + 2|E_3||E_4|\cos(\varphi_{34})\\ S_a^{(3)} &= 2|E_1||E_2|\sin(\varphi_{12}) + 2|E_3||E_4|\sin(\varphi_{34})\end{aligned} \tag{8}$$

and

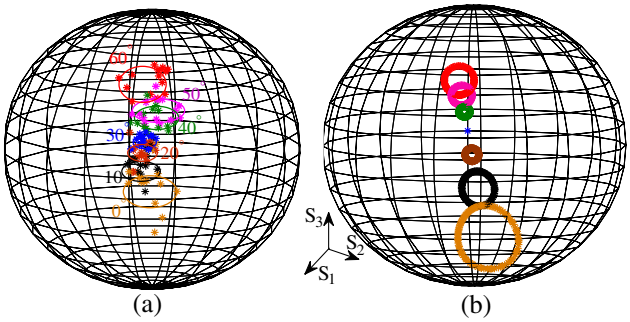

Fig. 3. (Color online) Poincaré sphere representation of the SOP at the output as a function of the wavelength for different angular orientations of the linear polarization at the input. (a) Experimental results and (b) calculated results. The input wavelength ranged from 1062 nm to 1066 nm for each angular orientation.

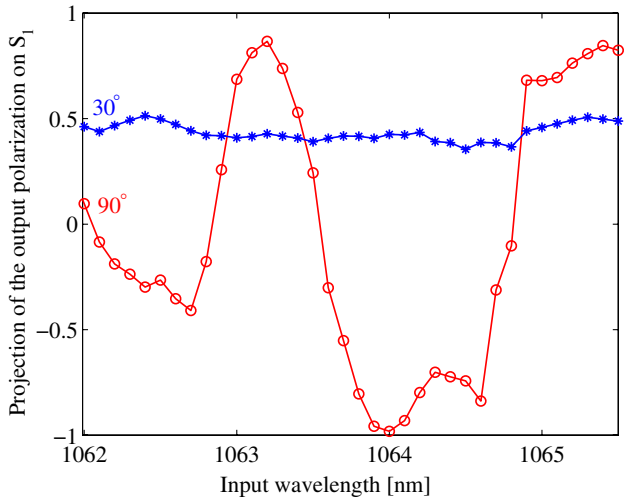

Fig. 4. (Color online) Projection of the output polarization on the S_1 axes as a function of the input wavelength for two orientations of the input polarization; asterisks (blue) 30° orientation, close to the PM; circles (red) 90° orientation, far from the PM.

$$\begin{aligned}S_b^{(1)} &= |E_1|^2 + |E_2|^2 - |E_3|^2 - |E_4|^2\\ S_b^{(2)} &= 2|E_1||E_3|\cos(\varphi_{13}) + 2|E_2||E_4|\cos(\varphi_{24})\\ S_b^{(3)} &= 2|E_1||E_3|\sin(\varphi_{13}) + 2|E_2||E_4|\sin(\varphi_{24}),\end{aligned} \tag{9}$$

where φ_{ij} denote the phase difference between E_i and E_j. Now, Eq. (1) can be separated into two uncoupled torque equations, as

$$\begin{aligned}\dot{S}_a &= \tau_a \times S_a\\ \dot{S}_b &= \tau_b \times S_b.\end{aligned} \tag{10}$$

Note, the torque vectors depend only on the parameters of the fiber and not on the input SOP so presenting the output SOP with these modified Poincaré spheres for different input SOP results in concentric circles, as presented in Fig. 5. Since the modified Poincaré spheres include both the polarization of the beam and the spatial distribution while the original Poincaré sphere includes only the polarization, it is possible to find from the modified Poincaré spheres the SOP in the original one but not vice-versa.

Using the two sets of modified Stokes parameters, we recalculated the evolution of the output SOP as a function of the input wavelength for different angular orientations of a linearly polarized light at the input. The results are presented in Fig. 6. As evident, the use of the modified Stokes parameters and the separation of Eq. (1) into two uncoupled equations, resulted in two modified Poincaré spheres where the SOPs in each sphere

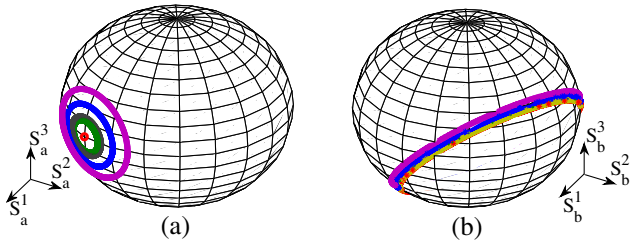

Fig. 5. (Color online) Calculated modified Poincaré sphere representation of the SOP at the output as a function of the wavelength for different angular orientations of linearly polarized light at the input. (a) Using the modified Stokes parameters S_a and (b) using the modified Stokes parameters S_b.

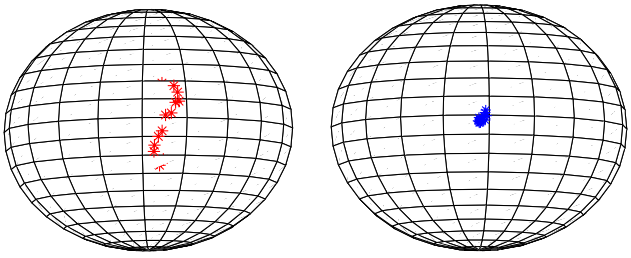

Fig. 6. (Color online) Average polarization when varying the input wavelength for different input polarizations on (a) the original Poincare sphere and on (b) the modified Poincare sphere.

form concentric, rather than displaced, circles around the PM when varying the input wavelength. The modified Poincaré spheres representations involve natural modes of a fiber. Specifically, S_a represents the modes TE_{01} and TM_{01}, and S_b represents the modes HE_{21} and HE_{-21}. These results indicate that when evaluating the propagation of light in multimode fiber it is preferable and more convenient to resort to our uncoupled modified Poincaré spheres representation rather than the usual Poincaré sphere representation [12,13].

Based on the calculated results from our model we reevaluated our experimental results in order to obtain more convenient and more intuitive Poincaré sphere representations of the SOP dynamics at the output from a multimode fiber. Specifically, we first multiplied the measured light distribution with those of the transverse modes shown in Fig. 2. Then we determine the SOP at each point across the beam, which leads to determining the contribution of the fields E_1, E_2, E_3, and E_4. Next, we used Eq. (8) to determine the modified Stokes parameters S_a to obtain the desired modified Poincaré sphere representation. For simplicity we present only the average SOP (center of circles) for each angular orientation of the linearly polarized input beam. The results are presented in Fig. 6. Figure 6(a) shows the average SOP for different input polarization orientations in the original Poincaré sphere representation, same as Fig. 3. Here, the average SOP is displaced as we vary the input polarization orientation. Figure 6(b) shows the corresponding results on the modified Poincaré sphere representation. As evident, here the average SOP is about the same for the different input polarization orientations, as expected.

5. CONCLUSION

To conclude, we presented experimental and calculated results about the dynamics of modes and their SOP in multimode fibers. We show how the representation of these dynamics can be simplified so as to obtain a direct measure of the SOP at the output when knowing the input SOP. The results of this measure can then be used for determining the SOP for an arbitrary input SOP. This method can be applied to any four modes that have nearest neighbor coupling or to high order modes fibers where the coupling between different modes has some symmetry so the coupling matrix is sparse. Then, the complicated multidimension dynamics can be reduced to simpler dynamics with lower dimension.

ACKNOWLEDGMENTS

This research was supported by the Israeli Ministry of Science and Technology and by the USA-Israel Binational Science Foundation.

REFERENCES

1. P. Pepeljugoski, M. J. Hackert, J. S. Abbott, S. E. Swanson, S. E. Golowich, A. J. Ritger, P. Kolesar, Y. C. Chen, and P. Pleunis, "Development of system specification for laser-optimized 50 μm multimode fiber for multigigabit short-wavelength LANs," J. Lightwave Technol. **21**, 1256–1275 (2003).
2. C. Lethien, C. Loyez, and J. P. Vilcot, "Potentials of radio over multimode fiber systems for the in-buildings coverage of mobile and wireless LAN applications," J. Lightwave Technol. **17**, 2793–2795 (2005).
3. J. P. Gordon and H. Kogelnik, "PMD fundamentals: Polarization mode dispersion in optical fibers," Proc. Natl. Acad. Sci. USA **97**, 4541–4550 (2000).
4. B. L. Heffner, "Automated measurement of polarization mode dispersion using Jones matrix eigenalysis," IEEE Photon. Technol. Lett. **4**, 1066–1069 (1992).
5. C. D. Poole and R. E. Wagner, "Phenomenological approach to polarisation dispersion in long single mode fibers," Electron. Lett. **22**, 1029–1030 (1986).
6. W. Shieh and H. Kogelnik, "Dynamic eigenstates of polarization," IEEE Photon. Technol. Lett. **13**, 40–42 (2001).
7. C. D. Poole, J. H. Winters, and J. A. Nagel, "Dynamical equation for polarization dispersion," Opt. Lett. **16**, 372–374 (1991).
8. D. Andrescianci, F. Curti, F. Matera, and B. Daino, "Measurement of the group-delay difference between the principal state of polarization on a low-birefringence terrestrial fiber cable," Opt. Lett. **12**, 844–846 (1987).
9. C. D. Poole, N. S. Bergano, R. E. Wagner, and H. J. Schulte, "Polarization dispersion and principal state in a 147 km undersea lightwave cable," J. Lightwave Technol. **6**, 1185–1190 (1988).
10. G. P. Agrawal, *Fiber-Optic Communication System*, 3rd ed. (Wiley, 2002).
11. S. Wielandy, "Implications of higher-order mode content in large mode area fibers with good beam quality," Opt. Express **15**, 15402–15409 (2007).
12. M. J. Padgett and J. Courtial, "Poincaré-sphere equivalent for light beams containing orbital angular momentum," Opt. Lett. **24**, 430–432 (1999).
13. G. S. Agarwal, "SU(2) structure of the Poincaré sphere for light beams with orbital angular momentum," J. Opt. Soc. Am. A **16**, 2914–2916 (1999).
14. S. Fan and J. M. Kahn, "Principal modes in multimode waveguides," Opt. Lett. **30**, 135–137 (2005).
15. M. B. Shemirani, W. Mao, R. A. Panicker, and J. M. Kahn, "Principal modes in graded-index multimode fiber in presence of spatial and polarization mode coupling," J. Lightwave Technol. **27**, 1248–1261 (2009).
16. M. Fridman, M. Nixon, M. Dubinskii, A. A. Friesem, and N. Davidson, "Principal modes in fiber amplifiers," Opt. Lett. **36**, 388–390 (2011).
17. M. Fridman, M. Nixon, E. Grinvald, N. Davidson, and A. A. Friesem, "Real-time measurement of unique space-variant polarizations," Opt. Express **18**, 10805–10812 (2010).
18. S. Ramachandran, P. Kristensen, and M. F. Yan, "Generation and propagation of radially polarized beams in optical fibers," Opt. Express **34**, 2525–2527 (2009).
19. M. Fridman, G. Machavariani, N. Davidson, and A. A. Friesem, "Fiber lasers generating radially and azimuthally polarized light," Appl. Phys. Lett. **93**, 191104 (2008).
20. R. Ulrich and A. Simon, "Polarization optics of twisted single mode fiber," Appl. Opt. **18**, 2241–2251 (1979).
21. D. M. Shyroki, "Exact equivalent straight waveguide model for bent and twisted waveguides," IEEE Trans. Microwave Theory Tech. **56**, 414–419 (2008).
22. H. Suchowski, Y. Silberberg, and D. B. Uskov, "Pythagorean coupling: Complete population transfer in a four-state system," Phys. Rev. A **84**, 013414 (2011).
23. P. Du Val, "Homographies, quaternions and rotations," in *Oxford Mathematical Monographs* (Clarendon, 1964).